Mapping Mechanical Properties on the Nanoscale Using Atomic-Force Acoustic Microscopy

D.C. Hurley, M. Kopycinska-Müller, and A.B. Kos

Tools are being developed that use the atomic-force microscope (AFM) to measure mechanical properties with nanoscale spatial resolution. Contact-resonance-spectroscopy techniques such as atomic-force acoustic microscopy involve the vibrational modes of the AFM cantilever when its tip is in contact with a material. These methods enable quantitative maps of local mechanical properties such as elastic modulus and thin-film adhesion. The information obtained furthers the understanding of patterned surfaces, thin films, and nanoscale structures.

INTRODUCTION

"In order to be widely used, future nanodevices will require nanomechanical measurements that are rapid, accurate, predictive, well-understood, and representative of a device or system's environment in real time."[1] This vision of the National Nanotechnology Initiative describes the general need for measurement tools for emerging nanotechnology applications, a field expected to create a multibillion-dollar market for materials within the next decade. It also emphasizes the specific need for nanomechanical information—knowledge on nanometer length scales of mechanical properties such as elastic modulus, strength, adhesion, and friction. This is because applications increasingly involve several disparate materials integrated on the micro- or nano-scale (e.g., electronic interconnects, nanocomposites). The complexity of fabricating such systems dictates the use of predictive modeling to save time and money. Yet modeling can correctly predict system performance only if the property data used as input are accurate at the relevant length scales. In addition to the achievement of nanoscale spatial resolution, there is a growing need to visualize the spatial distribution in properties instead of relying on a single "average" value. In such heterogeneous systems it is frequently the localized variation or divergence in properties that causes failure (void formation, fracture, etc.). Engineering these complex systems thus requires quantitative nanomechanical imaging to better predict reliability and performance.

Methods that show the most promise for quantitative information are dynamic approaches in which the cantilever is vibrated at or near its resonant frequencies.

Many methods to obtain small-scale mechanical-property data[2–5] have drawbacks. For instance, nanoindentation (NI)[2] is inherently destructive, with each measurement creating an indent hundreds to thousands of nanometers wide. In addition, the spatial resolution afforded by conventional NI techniques may not be sufficient as dimensions shrink further and very compliant materials are increasingly used. A promising method combines low-load NI techniques with force modulation and scanning.[3] However, the lateral resolution is still limited by the radius (a few hundred nanometers) of the Berkovich diamond indenter used.

Methods that use the atomic-force microscope (AFM) present an attractive alternative for characterizing mechanical properties. The AFM's scanning ability and the small radius (typically 5 nm to 50 nm) of the cantilever tip enable rapid, in-situ imaging with nanoscale spatial resolution. The AFM was originally created to measure surface topography with atomic spatial resolution;[6] since then, a variety of AFM techniques to sense mechanical properties have been demonstrated.[7–10] Methods that show the most promise for quantitative information are dynamic approaches in which the cantilever is vibrated at or near its resonant frequencies.[11] Although more appropriately called contact-resonance-spectroscopy methods, variations are often labeled acoustic or ultrasonic corresponding to the characteristic vibrational frequencies involved (~100 kHz to 3 MHz). Among them are ultrasonic-force microscopy (UFM),[12] heterodyne-force microscopy,[13] ultrasonic atomic-force microscopy (UAFM),[14] and atomic-force acoustic microscopy (AFAM).[15]

This article describes work toward quantitative measurements and imaging of nanoscale mechanical properties with contact-resonance-spectroscopy methods, in particular, AFAM.

See the sidebar for a description of the principles of contact-resonance spectroscopy.

SINGLE-POINT MODULUS MEASUREMENTS WITH AFAM

Experiments using AFAM concepts are performed with an apparatus such as

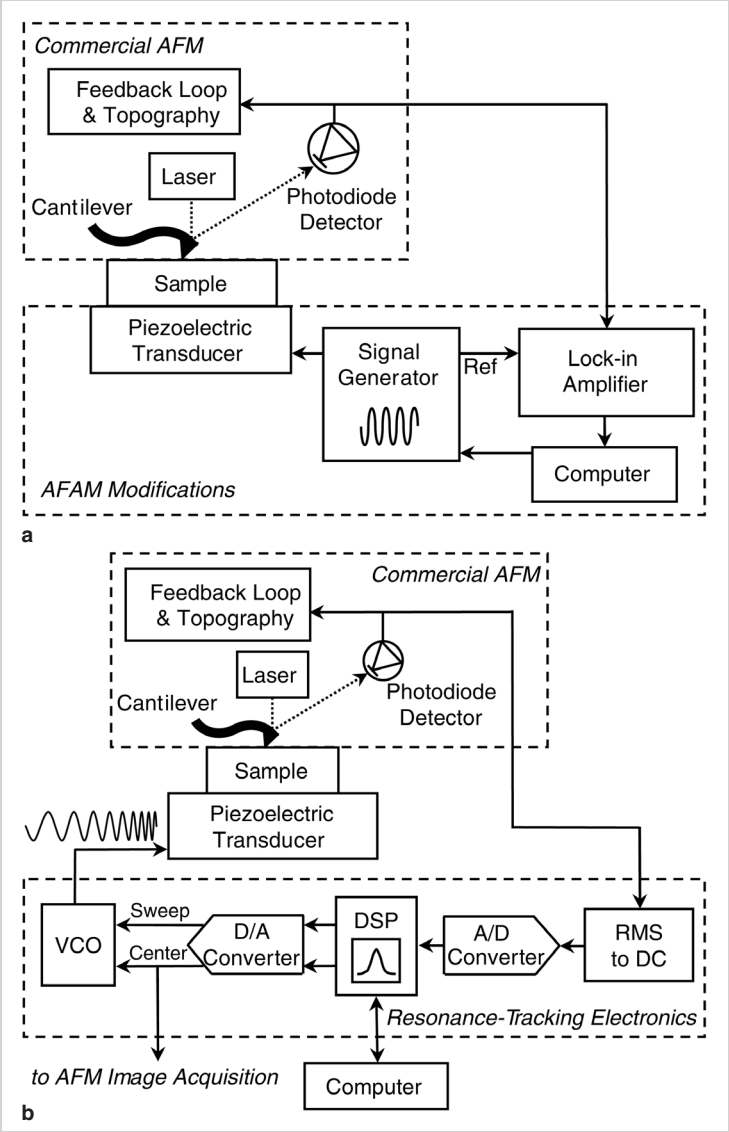

Figure 1. The schematics of experimental apparatus used for (a) AFAM modulus measurements at a fixed sample position and (b) contact-resonance-frequency imaging.

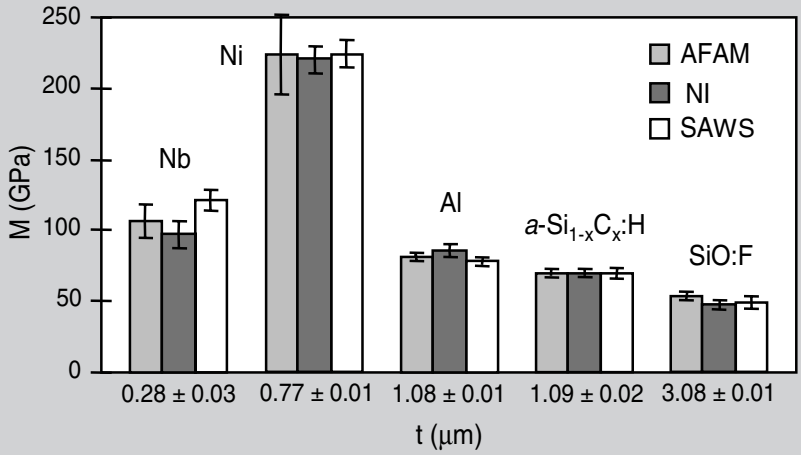

Figure 2. The indentation modulus M of thin supported films obtained by AFAM, nanoindentation (NI), and surface acoustic wave spectroscopy (SAWS). The thickness t of each film was determined by cross-sectional scanning-electron microscopy analysis or by stylus profilometer methods. Film materials include fluorinated silica glass (SiO:F), amorphous hydrogenated silicon carbide (a-$Si_{1-x}C_x$:H), aluminum, niobium, and nickel. The error bars represent the standard deviation due to scatter of multiple measurements.

Equations

$$k^* = \sqrt[3]{6F_C R E^{*2}} \quad (1)$$

$$\frac{1}{E^*} = \frac{1}{M_{tip}} + \frac{1}{M_s} \quad (2)$$

$$E^*_s = E^*_{ref}\left(\frac{k^*_s}{k^*_{ref}}\right)^n \quad (3)$$

the one shown schematically in Figure 1a. The apparatus is based on a standard, commercially available AFM with a few additional off-the-shelf instruments. Note that access to the unfiltered photodiode output signal from the AFM is required. For AFAM measurements, the specimen is bonded to an ultrasonic piezoelectric transducer mounted on the AFM translation stage. The transducer is excited with a continuous sine wave voltage by a function generator. The amplitude of the cantilever deflection is monitored by the AFM's internal position-sensitive photodiode. Lock-in techniques are used to isolate the component of the photodiode signal at the excitation frequency. In this way, a spectrum of the cantilever response versus frequency can be obtained by sweeping the transducer excitation frequency and recording the lock-in output signal.

Contact-resonance spectra are acquired for transducer excitation voltages sufficiently low that the tip-sample interaction remains linear. As described in the sidebar, spectra for two different resonant modes are needed in order to determine the effective tip position L_1. Most commonly, the two lowest flexural (bending) modes are used, although torsional and lateral modes have also been examined.[20] Frequency measurements are made on two samples in alternation: the test or unknown sample and a reference or calibration specimen whose elastic properties have been determined by another means. The measured contact-resonance frequencies are used to calculate values of k* for both the test and reference materials with the beam-dynamics model mentioned in the sidebar. From the calculated values of k^*_{ref} and k^*_s and independent knowledge of the reference material's elastic properties, the reduced Young's modulus E^*_s for the unknown specimen can be cal-

culated by Equation 3,[24] where E^*_{ref} is the reduced Young's modulus of the reference material (all equations are listed in the Equations table). The exponent n depends on the model used to describe the contact mechanics between the tip and sample.[22] Usually, a spherical (n = 3/2) or flat-punch (n = 1) tip geometry is assumed. The indentation modulus M_s of the test sample is then determined from E^*_s using Equation 2 and knowledge of M_{tip}. Multiple data sets are obtained by comparing measurements on the unknown sample to those made on the reference sample immediately before and afterward. Averaging the data sets yields a single value for the indentation modulus of the test material, M_s, for which the effects of tip wear are minimized.

Comparison measurements with a reference material of known elastic properties eliminate the need for precise knowledge of the tip radius R (see Equation 1), which is very difficult to determine directly. The use of multiple reference samples has also been demonstrated as a way to improve measurement accuracy.[18,25] Because k* depends on the contact area, the comparison method relies on the assumption that the contact geometry is identical for the test and reference materials. An alternative approach that avoids this assumption by means of a tip shape estimation procedure has also been developed.[26]

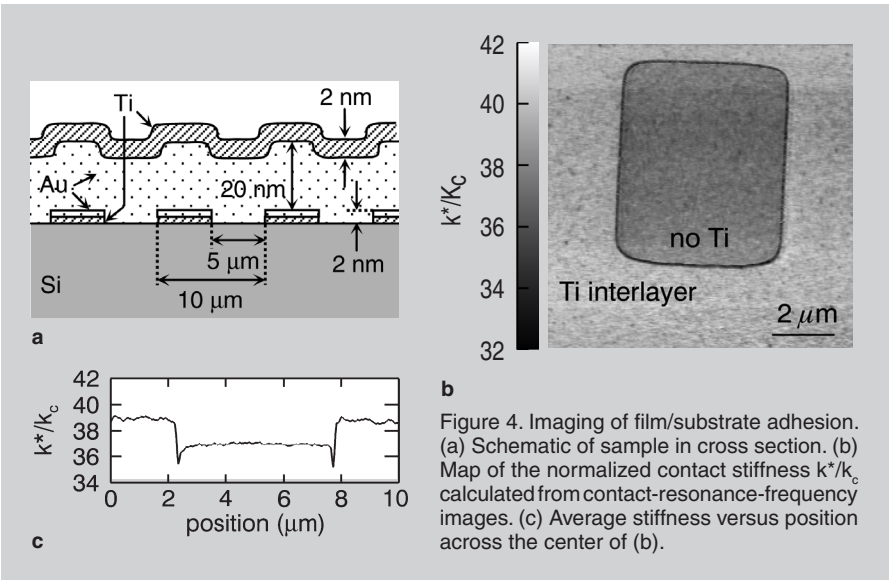

Figure 4. Imaging of film/substrate adhesion. (a) Schematic of sample in cross section. (b) Map of the normalized contact stiffness k^*/k_c calculated from contact-resonance-frequency images. (c) Average stiffness versus position across the center of (b).

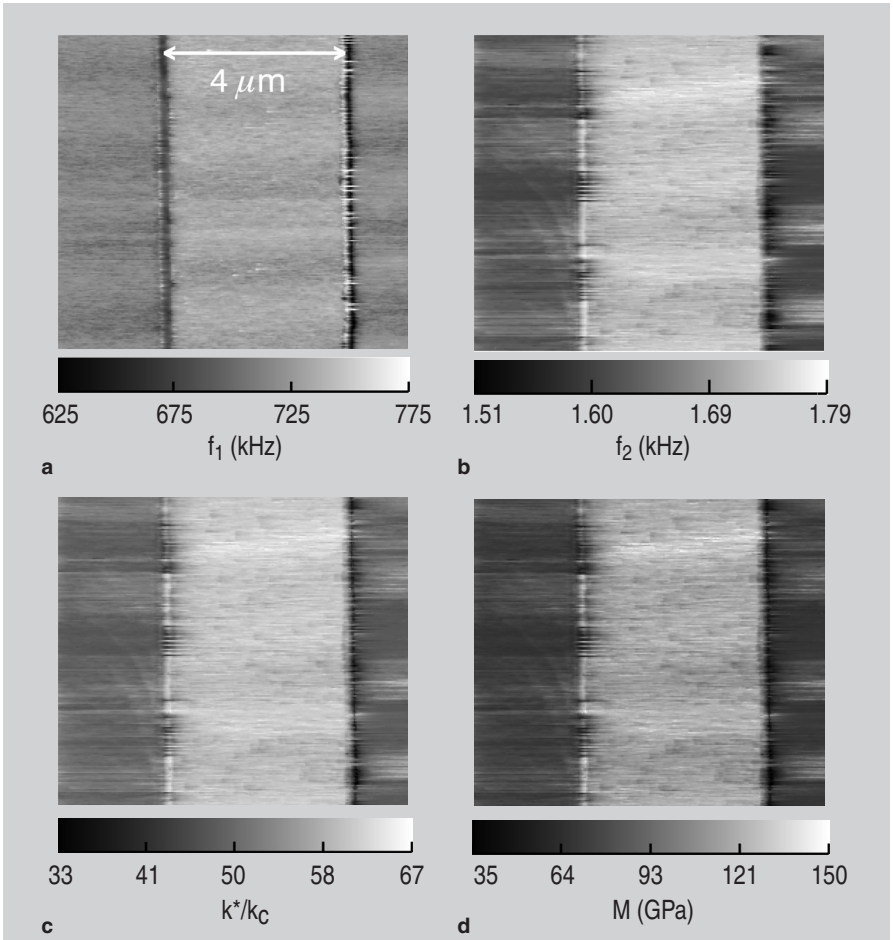

Figure 3. Quantitative AFAM images for an Nb/SiO_2 thin-film sample. Contact-resonance frequency images of (a) first (f_1) and (b) second (f_2) flexural modes, respectively. (c) Normalized contact stiffness k^*/k_c calculated from (a) and (b). (d) Map of indentation modulus M calculated from (c) assuming Hertzian contact mechanics.

The accuracy of this experimental approach has been examined by comparing AFAM measurements with values obtained by other techniques.[18,27] Figure 2 shows the results of such experiments. Measurements of the indentation modulus M were made on thin supported films of several different materials with AFAM, NI, and surface acoustic wave spectroscopy (SAWS). As mentioned previously, NI is destructive to the sample and has somewhat poorer spatial resolution than AFAM, but is widely used in industry. The SAWS method[5] is used primarily in research laboratories; although nondestructive, the values obtained represent the average sample properties over a few square centimeters. Figure 2 shows that the results from all three methods are in very good agreement (differences of less than 10% and within the measurement uncertainty) for all of the samples.

Results such as these demonstrate the validity of AFAM methods for quantitative determination of elastic properties. Additional research is ongoing both to improve measurement precision and accuracy and to more fully understand the extent to which the methods can be applied. For example, the effect of film thickness on AFAM measurement accuracy was examined with a series of nanocrystalline nickel films deposited on silicon substrates.[28] The results indi-

cated that for nickel films even as thin as about 50 nm, AFAM measures the properties of the film alone and is not affected by the properties of the substrate. The film thickness for which the substrate begins to play a role depends on the elastic properties of both the tip and sample. In addition, recent studies have begun to delve more deeply into the true nature of the nanoscale contact mechanics between the tip and sample.[29,30] Other research involves efforts to include the effects of a damping (inelastic) term in the tip-sample contact, due, for instance, to capillary forces from thin surface layers.[31] Further work is needed to incorporate the results of such studies into an improved AFAM procedure for quantitative measurements.

STIFFNESS IMAGING AND MAPPING

Contact-resonance spectroscopy methods may also be used for two-dimensional imaging of near-surface mechanical properties. Qualitative "amplitude images" indicative of local variations in stiffness[16,32] are obtained with an apparatus like that in Figure 1a and a fixed excitation frequency. As the tip is scanned across the sample, the lock-in detector senses variations in the cantilever vibration amplitude caused by changes in the local stiffness. The output signal of the lock-in is used as an external input to the AFM for imaging. Amplitude imaging has been used to investigate the nanoscale elastic properties of systems such as piezoelectric ceramics,[15] carbon-fiber-reinforced polymers,[16] and dislocations in graphite.[33]

Correct interpretation of amplitude images is difficult,[20] especially for material systems with several phases or components. More useful are nanomechanical maps—quantitative images of nanoscale properties. To obtain such maps, it is necessary to rapidly detect the contact-resonance frequency at each point on the sample as the tip is scanned. Recently, several approaches have been demonstrated to achieve contact-resonance frequency imaging.[14,15,34] Now maps of frequency, contact stiffness, and modulus[27,35] are emerging as tools for materials characterization.

In contrast to other methods, the authors' approach to contact-resonance frequency imaging is based on a digital signal processor (DSP) architecture.[27] A DSP approach facilitates future upgrades because changes are made in software instead of hardware. A schematic of the frequency-tracking apparatus is shown in Figure 1b. The circuit applies a swept-frequency sinusoidal voltage to the piezoelectric transducer. The AFM photodiode signal is converted to a direct current (DC) voltage proportional to the root mean square (rms) amplitude of vibration (rms-to-DC converter, bandwidth from 1 kHz to 3.2 MHz) and supplied to an analog-to-digital (A/D) converter. From the rms voltage versus frequency response, the circuit constructs a resonance spectrum and finds its peak. A digital feedback control loop uses this information to adjust a voltage-controlled oscillator so that the frequency sweep window remains centered on the contact-resonance frequency as it changes with sample position. The control voltage is also sent to the AFM through an auxiliary image channel. The acquired voltage image thus represents the value of the contact-resonance frequency at each position. With the specific circuit components used, the current system acquires a complete 128-point cantilever resonance spectrum every 2.7 ms (375 Hz repetition rate). The AFM scan speed must be adjusted to ensure that several spectrum sweeps are made at each image position. For scan lengths up to several micrometers, an image with 256×256 pixels is usually acquired in less than 25 min.

Results obtained with contact-resonance-frequency imaging techniques are shown in Figure 3. The sample contained a silica (SiO_2) blanket film (thickness ~350 nm) deposited on a silicon wafer.

PRINCIPLES OF CONTACT-RESONANCE SPECTROSCOPY

Contact-resonance spectroscopy techniques—methods that use the resonant modes of the atomic-force microscope (AFM) cantilever in order to evaluate near-surface mechanical properties—have been utilized by several groups.[15–18] For clarity, the discussion here is limited to the atomic-force acoustic microscopy (AFAM) technique first developed by U. Rabe and coworkers.[15,19,20] The basic concepts of AFAM are shown in Figure A. Resonant vibrational modes of the cantilever are excited by either the built-in piezoelectric element of the AFM cantilever holder or by an external actuator such as an ultrasonic transducer. When the tip of the cantilever is in free space, as in Figure Aa, the resonant modes occur at specific frequencies that depend on the geometry and material properties of the cantilever. When the tip is placed in contact with a specimen as in Figure Ab, the frequencies of the resonant modes increase due to tip-sample forces that stiffen the system, as illustrated schematically in Figure Ac. Atomic-force acoustic microscopy and other contact-resonance-spectroscopy methods exploit the fact that mechanical properties of the sample can be deduced by measuring these "free-space" and "contact-resonance" frequencies and interpreting them with suitable models.

The first model needed to interpret contact-resonance spectra involves the dynamics of the vibrating cantilever. Both analytical[19,20] and finite-element[18,21] analysis approaches have been used. The simplest model to describe the interaction, shown in Figure Ad, contains a rectangular cantilever beam of length L and stiffness k_c. The cantilever is coupled to the sample by a spring of stiffness k* that represents a purely elastic interaction. This approximation is valid if the applied load F_c is much greater than the adhesive force but low enough to avoid plastic deformation of the sample. These conditions are valid under typical experimental conditions involving relatively stiff materials (e.g., metals and ceramics) and stiff cantilevers (spring constant k_c approximately 40 N/m to 50 N/m) for which $F_c \approx 0.4\ \mu N$ to $2\ \mu N$.

The analytical model for beam dynamics provides a characteristic equation that links the measured frequencies to the tip-sample contact stiffness k*. If the model assumes that the AFM tip is located at the very end of the cantilever, the values of k* obtained with this equation for different contact-resonance modes are usually not equal. To insure that the value of k* is the same regardless of mode, the model includes an adjustable tip position parameter $L_1 < L$,[19,20] as indicated in Figure Ad. In this case, k* is calculated as a function of the tip position L_1 for each resonant mode. The position at which k* is the same for the two modes is taken as the solution. Typical values of the effective tip position are $L_1/L \approx 0.94$ to 0.98. These values are consistent with scanning-electron measurements of actual cantilever dimensions.[18]

The values of k* are used to calculate the elastic properties of the sample with the

On top of the SiO_2 film was a niobium strip (~180 nm thick × 4 μm wide). Contact-resonance frequency images are shown in Figure 3a and b for the first (f_1) and second (f_2) flexural modes, respectively. The narrow, bright, and dark vertical lines indicate relatively large, spurious frequency changes that occur from sudden changes in the tip-sample contact area at the edges of the niobium strip. Otherwise, the frequency values for the individual materials are uniform and repeatable from line to line. It is clear that the average contact-resonance frequencies of the central niobium strip are greater than those of the SiO_2 film regions to the left and right.

An image of the normalized contact stiffness k^*/k_c calculated from the images of f_1 and f_2 is shown in Figure 3c. The image was calculated from the contact-resonance-frequency images on a pixel-by-pixel basis with the AFAM point approach described. To calculate a map of the indentation modulus M from the contact-stiffness image, Hertzian contact mechanics were used and it was assumed that the mean value of k^*/k_c for the SiO_2 region corresponded to $M_{SiO2} = 75.1$ GPa. This value of M was obtained from AFAM fixed-point measurements made on the SiO_2 film using bulk fused silica as the reference sample. The resulting modulus map is shown in Figure 3d. The mean value for M in the entire SiO_2 region is $M_{SiO2} = 75.5 \pm 7.1$ GPa, while the mean value for the niobium film region is $M_{Nb} = 118.5 \pm 7.1$ GPa. These results are consistent with the values $M_{SiO2} = 72$ GPa to 77 GPa and $M_{Nb} = 116$ GPa to 133 GPa given in the literature for the bulk materials. They also agree with AFAM point measurements that yielded $M_{Nb} = 112.7 \pm 15.0$ GPa. Furthermore, the relatively small standard deviation of the values (5% to 10%) indicates that the tip-sample contact is consistent and repeatable.

help of a second model for the tip-sample contact mechanics.[22] Most commonly used are Hertzian contact mechanics, which describe the elastic interaction between a hemispherical tip of radius R pressed against a flat surface with an applied force F_c. In this case, k* is determined by Equation 1. (Note: All equations appear in the Equations table.) Here E* is the reduced Young's modulus, defined by Equation 2 where M_s and M_{tip} correspond to the indentation moduli of the sample and the AFM tip, respectively. For elastically isotropic materials $M = E/(1-\nu^2)$, where E is Young's modulus and ν is Poisson's ratio. In anisotropic materials, M depends on direction and is calculated from the second-order elastic stiffness tensor.[23]

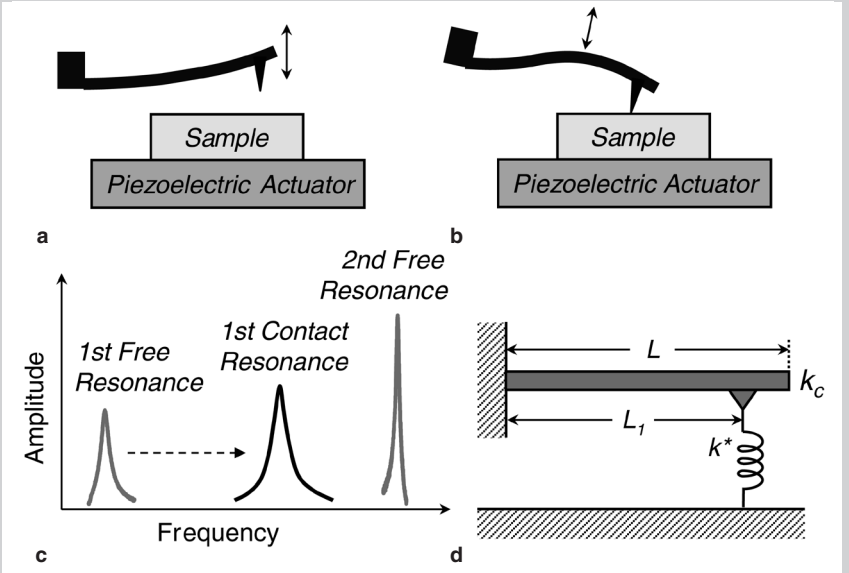

Figure A. Concepts of AFAM contact-resonance spectroscopy. Resonant modes of the cantilever are excited by a piezoelectric actuator mounted beneath the sample when the tip is (a) in free space and (b) in contact with the sample. Flexural (bending) modes of the cantilever are illustrated here. (c) Resonant spectra. The first contact resonance [shown in (b)] occurs at a higher frequency than the first free-space resonance [shown in (a)], but is lower than the second free-space resonance. (d) An AFAM beam-dynamics model. A rectangular cantilever beam with stiffness k_c is clamped at one end and has a total length L. It is coupled to the surface through a spring of stiffness k* (contact stiffness) located at a position L_1 with respect to the clamped end.

APPLICATIONS OF CONTACT-RESONANCE IMAGING

Only recently have contact-resonance-spectroscopy techniques blossomed into valuable tools for nanoscale materials characterization. Recent results for two different applications illustrate the potential of these techniques. The first example concerns the interfacial adhesion between a thin film and its underlying substrate.[36] In the second study, the elastic properties of tin oxide nanobelts are examined.[37]

Contact-resonance-spectroscopy methods can be used to evaluate other mechanical properties besides elastic modulus if they influence the contact stiffness between the tip and the sample. One such property of technological interest is the relative bonding or adhesion between a film and a substrate. To experimentally investigate the sensitivity of these methods to variations in film adhesion,[36] the authors fabricated a model system of gold and titanium films on (001) silicon. Figure 4a shows a cross-sectional schematic of the sample. A rectangular array of 5 μm × 5 μm squares (10 μm pitch) of Au/Ti surrounded by a grid of Ti/Au/Ti was fabricated on silicon by standard microfabrication techniques. The sample was intended to contain variations in the adhesion of a buried interface with only minimal variations in topography and composition at the surface. A crude scratch test was performed by lightly dragging one end of a tweezer across the sample. Optical micrographs showed that this treatment had removed the film in the scratched regions without a titanium interlayer (squares) and left the gold intact in the scratched regions containing a titanium interlayer (grid). The result confirmed the expectation that the film adhesion was much stronger in regions containing the titanium interlayer. The titanium topcoat was included merely to prevent contamination of the AFM tip by the soft gold film.

To understand how AFAM senses variations in a buried interface, note that experiments probe the sample properties to a depth z roughly three times that of

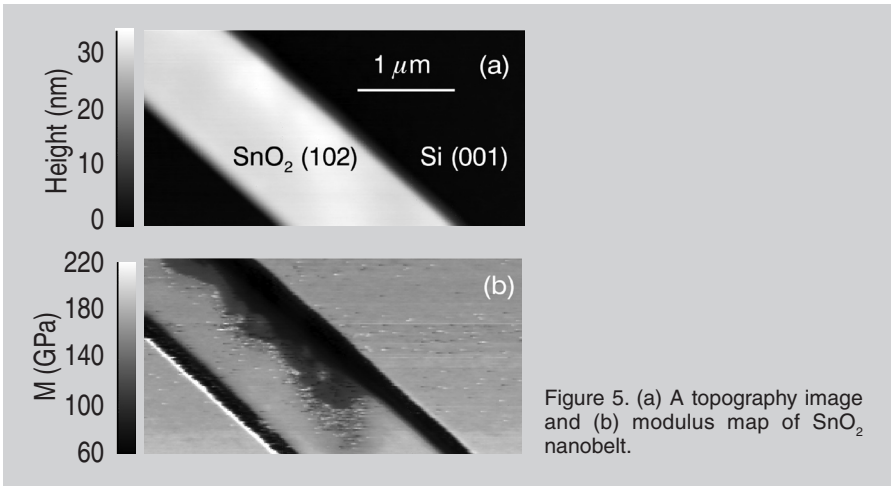

Figure 5. (a) A topography image and (b) modulus map of SnO_2 nanobelt.

the tip-sample contact radius a.[22] For Hertzian contact mechanics, $a^3 = (3RF_c)/(4E^*)$. For $z > 3a$, the stress field beneath the tip is sufficiently small relative to the value at the surface (<10%) that the measurement is not sensitive to property variations. In this way, the relative depth sensitivity of methods such as AFAM is affected by the choice of experimental parameters R and F_c. Using the above equation, the authors estimate that a = 6 nm to 8.5 nm for the experimental parameters. Therefore, the experiments should probe the film interface (z = 22 nm to 24 nm ≈ 3a).

Contact-resonance-frequency imaging experiments were performed on the sample with the methods described. An image of the normalized contact stiffness k^*/k_c calculated from the experimental contact-resonance frequency images of f_1 and f_2 is shown in Figure 4b. The image reveals that the contact stiffness is lower in the square region with poor adhesion (no titanium interlayer). A line scan of the average value of k^*/k_c versus position obtained from 40 lines in the center of the image is shown in Figure 4c. The mean value of k^*/k_c is 39.1 ± 0.6 in the grid regions and 37.1 ± 0.5 in the square, a difference of 5%. Several other contact-stiffness images acquired at different sample positions consistently showed a decrease of 4% to 5% in k^*/k_c for the regions of poor adhesion that lacked a titanium interlayer.

The results are consistent with theoretical predictions for layered systems with disbonds.[38] An impedance-radiation theory modeled the disbonded substrate/film interface by a change in boundary conditions (i.e., zero shear stress at the interface). For a disbond in a 20 nm aluminum film (M = 78 GPa) on (001) silicon (M = 165 GPa), a reduction of approximately 4% in the contact stiffness was predicted, very similar to the described results. The system modeled in Reference 38 contained a different film material than used in these experiments. However, the overall combination of conditions (film and substrate modulus, applied force, etc.) was sufficiently similar to the authors' that a comparison is valid. These results represent progress toward quantitative imaging of adhesion, a goal with important implications for the development of thin-film devices in many technological applications.

In another application, tin oxide (SnO_2) nanobelts were examined with contact-resonance methods.[37] Quasi-one-dimensional structures such as nanotubes, nanowires, and nanobelts are subject to much research interest due to the promise they show for new nanoscale devices. Because such devices are still in the earliest stages of development, fundamental materials-property data for the component materials are needed. However, the spatial resolution of many conventional methods is simply inadequate for these nanoscale structures. For this reason, AFM methods are an attractive option.

Nanobelts were synthesized by heat treatment of tin powder in a quartz tube furnace. The nanobelts formed by this method were removed from the alumina substrates and deposited on (001) silicon substrates by solvent methods. Ion-milling techniques were used to mark the substrate near specific nanobelts of interest so that they could be reliably identified. Topogaphic images obtained with contact AFM methods indicated that the nanobelts were typically 0.5 μm to 1.0 μm wide, 30 nm to 50 nm high, and several tens of micrometers in length. Electron-backscatter-diffraction analysis indicated that the crystalline structure of the nanobelts was tetragonal, as expected for single-crystal SnO_2. The nanobelts studied in this work had a surface normal parallel to the (102) reciprocal lattice vector. Auger-electron spectroscopy revealed that the chemical composition of the nanobelts was the same as that of bulk SnO_2.

Several nanobelts were examined both by single-point modulus measurements and contact-resonance modulus mapping. The (001) silicon substrate was used as the reference material, with the value $M_{Si(100)}$ = 165 GPa used. Values for the indentation modulus M_{nb1} = 154 ± 18 GPa and M_{nb2} = 184 ± 13 GPa were obtained for two nanobelts from the single-point measurements. In these experiments, the Hertzian stress field penetration was estimated to be 45 nm to 60 nm, equal to or slightly greater than the nanobelt thickness. Thus a contribution to the measurement from the silicon substrate is possible. However, the AFAM results are in good agreement with the value M_{nb1} = 151 ± 14 GPa obtained with differential UFM,[37] which used sufficiently low forces that the substrate was not interrogated. Therefore, the effect of the substrate on the measurement was not considered to be substantial. The measured values are significantly lower than the value of 358 GPa calculated for (102) SnO_2 from the second-order elastic tensor. However, the results are consistent with other experimental and theoretical findings that report nanobelt modulus values significantly lower (up to 75%) than that of bulk SnO_2.[37] The reason for these finite-size effects is still under investigation.

Figure 5 shows results from contact-resonance imaging experiments on the nanobelt previously identified as #1. A topography image is given in Figure 5a, while Figure 5b contains the corresponding modulus map. Two contact-resonance frequency images were acquired and an image of the normalized contact stiffness k^*/k_c was calculated. The contact-stiffness image was converted to a modulus map using the mean value of k^*/k_c in the silicon region of the image

as a reference. Darker areas can be seen at the right-hand edges of the nanobelt. At first impression, this suggests that these areas have a lower modulus. However, the authors believe they actually represent regions of reduced contact stiffness due to contamination between the nanobelt and the substrate. This hypothesis was formed from analysis of the sample topography. Although not clear in the image, individual topography line scans reveal that these areas are slightly taller (~3 nm to 5 nm) than the rest of the nanobelt. Like the thin-film adhesion effects discussed previously, contamination could cause variations in the nanobelt-substrate contact, which would appear as a reduction in contact stiffness. Averaging over the entire nanobelt region of the image including the dark regions yields a mean modulus value M_{nb} = 145 ± 28 GPa. If the dark regions are omitted, the mean is M_{nb} = 164 ± 10 GPa. These results are consistent with the described point measurements within the measurement uncertainty.

CONCLUSIONS AND OUTLOOK

Knowledge of mechanical properties at the nanoscale will be essential to the successful development of new nanoscale materials and structures. The results discussed here, as well as others from groups worldwide, show significant progress in advancing the state of the art. However, true quantitative nanomechanical imaging requires further research efforts. A deeper understanding of the dynamics of nonideal AFM cantilever beams as the tip interacts with the sample is needed for improved data analysis. To increase measurement accuracy and repeatability, it is important to better understand and control issues such as surface topography, wear of the silicon tip, and the actual tip-sample contact mechanics. Resolving such issues will result in refinements to contact-resonance-spectroscopy techniques and thus enhance their value as a quantitative measurement tools. It is anticipated that these types of dynamic AFM techniques will continue to develop and will play a crucial role in future nanotechnology efforts by providing quantitative nanomechanical information.

ACKNOWLEDGEMENTS

The authors thank W. Arnold, S. Hirsekorn, U. Rabe (Fraunhofer Institut für zerstörungsfreie Prüfverfahren, Saarbrücken, Germany), and J. Turner (University of Nebraska–Lincoln) for valuable interactions. The nanoindentation measurements were provided by N. Jennett (National Physical Laboratory, United Kingdom), A. Rar (University of Tennessee–Knoxville), and D. Smith (National Institute of Standards and Technology [NIST]). The SnO_2 nanobelt experiments were performed in collaboration with Y. Zheng and R. Geer (College of Nanoscale Science and Engineering, Albany, New York), who also provided those samples and performed the supplemental characterization. We are grateful to G. Pharr (University of Tennessee–Knoxville), Y. Dzenis (University of Nebraska–Lincoln), N. Barbosa, P. Dresselhaus, G. Hilton, E. Langlois, W. Rippard, and S. Russek (NIST) for providing the samples used in this work. The essential contributions of other current and former NIST coworkers (M. Fasolka, R. Geiss, D. Julthongpiput, R. Keller, J. Müller, and P. Rice) are also acknowledged.

References

1. *Instrumentation and Metrology for Nanotechnology,* Report of the National Nanotechnology Initiative Workshop (27–29 January 2004, Gaithersburg, MD); available at *www.nano.gov/NNI_Instrumentation_Metrology_rpt.pdf* .
2. W.C. Oliver and G.M. Pharr, *J. Mater. Res.,* 7 (6) (1992), pp. 1564–1583.
3. S.A. Syed Asif et al., *J. Appl. Phys.,* 90 (3) (2001), pp. 1192–1200.
4. O. Kraft and C.A. Volkert, *Adv. Engng. Mater.,* 3 (3) (2001), pp. 99–110.
5. A.G. Every, *Meas. Sci. Technol.,* 13 (5) (2002), pp. R21–R39.
6. G. Binning et al., *Phys. Rev. Lett.,* 56 (9) (1986), pp. 930–933.
7. P. Maivald et al., *Nanotechnology,* 2 (2) (1991), pp. 103–106.
8. M. Troyon et al., *Nanotechnology,* 8 (4) (1997), pp. 1630–171.
9. N.A. Burnham et al., *J. Vac. Sci. Technol. B.,* 14 (2) (1996), pp. 794–799.
10. A. Rosa-Zeiser et al., *Meas. Sci. Technol.,* 8 (11) (1997), pp. 1333–1338.
11. Q. Zhong et al., *Surface Science,* 290 (1-2) (1993), pp. L688–L692.
12. R.E. Geer et al., *J. Appl. Phys.,* 91 (7) (2002), pp. 4549–4555.
13. M.T. Cuberes et al., *J. Phys. D: Appl. Phys.,* 33 (19) (2000), pp. 2347–2355.
14. K. Yamanaka et al., *Appl. Phys. Lett.,* 78 (13) (2001), pp. 1939–1941.
15. U. Rabe et al., *J. Phys. D: Appl. Phys.,* 35 (20) (2002), pp. 2621–2635.
16. K. Yamanaka and S. Nakano, *Appl. Phys., A* 66 (1) (1998), pp. S313–S317.
17. K.B. Crozier et al., *Appl. Phys. Lett.,* 76 (14) (2000), pp. 1950–1952.
18. D.C. Hurley et al., *J. Appl. Phys.,* 94 (4) (2003), pp. 2347–2354.
19. U. Rabe et al., *Ultrasonics,* 38 (1-8) (2000), pp. 430–437.
20. U. Rabe, "Atomic Force Acoustic Microscopy," *Applied Scanning Probe Methods II*, ed. B. Bushan and H. Fuchs (New York: Springer, 2006), pp. 37–90.
21. R. Arinero and G. Lévêque, *Rev. Sci. Instr.,* 74 (1) (2003), pp. 104–111.
22. K.L. Johnson, *Contact Mechanics* (Cambridge, U.K.: Cambridge University Press, 1985), pp. 84–99.
23. J.J. Vlassak and W.D. Nix, *Phil. Mag. A,* 67 (5) (1993), pp. 1045–1056.
24. U. Rabe et al., *Surf. Interface Anal.,* 33 (2) (2002), pp. 65–70.
25. M. Prasad et al., *Geophys. Res. Lett.,* 29 (8) (2002), pp. 1172 1–4.
26. K. Yamanaka et al., *Rev. Sci. Instr.,* 71 (6) (2000), pp. 2403–2408.
27. D.C. Hurley et al., *Meas. Sci. Technol.,* 16 (11) (2005), pp. 2167–2172.
28. M. Kopycinska-Müller et al., *Nanotechnology,* 16 (6) (2005), pp. 703–709.
29. D. Passeri et al., *Rev. Sci. Instr.,* 76 (9) (2005), pp. 093904 1–6.
30. M. Kopycinska-Müller et al., *Ultramicroscopy,* 106 (6) (2006), pp. 466–474.
31. D.C. Hurley et al., *Appl. Surf. Sci.,* 253 (3) (2006) pp. 1274–1281.
32. U. Rabe et al., *J. Vac. Sci. Technol. B,* 15 (4) (1997), pp. 1506–1511.
33. T. Tsuji and K. Yamanaka, *Nanotechnology,* 12 (3) (2001), pp. 301–307.
34. D. Passeri et al., *Appl. Phys. Lett.,* 88 (12) (2006), pp. 121910 1–3.
35. T. Tsuji et al., *Appl. Phys. Lett.,* 87 (7) (2005), pp. 071909 1–3.
36. D.C. Hurley et al., *Appl. Phys. Lett.,* 89 (2) (2006), pp. 021911 1–3.
37. Y. Zheng et al., *J. Appl. Phys.*, in press (2006).
38. A.F. Sarioglu et al., *Appl. Phys. Lett.,* 84 (26) (2004), pp. 5368–5370.

D.C. Hurley, M. Kopycinska-Müller, and A.B. Kos are currently with the National Institute of Standards and Technology, 325 Broadway, Boulder, Colorado 80305-3328 USA. D.C. Hurley can be reached by e-mail at hurley@boulder.nist.gov.